

Article

Microstructure, Mechanical Properties, and Corrosion Resistance of Thermomechanically Processed AlZn6Mg0.8Zr Alloy

Aleksander Kowalski ^{1,*}, Wojciech Ozgowicz ², Wojciech Jurczak ³, Adam Grajcar ²,
Sonia Boczek ⁴ and Janusz Żelechowski ⁴

¹ Institute of Non-Ferrous Metals, 5 Sowińskiego Street, 44-100 Gliwice, Poland

² Silesian University of Technology, Institute of Engineering Materials and Biomaterials, 18A Konarskiego Street, 44-100 Gliwice, Poland; wojciech.ozgowicz@tlen.pl (W.O.); adam.grajcar@polsl.pl (A.G.)

³ Polish Naval Academy, Faculty of Mechanical and Electrical Engineering, 69 Śmidowicza Street, 81-127 Gdynia, Poland; w.jurczak@amw.gdynia.pl

⁴ Institute of Non-Ferrous Metals, Light Metals Division, 19 Piłsudskiego Street, 32-050 Skawina, Poland; sboczek@imn.skawina.pl (S.B.); jzelechowski@imn.skawina.pl (J.Ż)

* Correspondence: aleksander.kowalski@imn.gliwice.pl; Tel.: +48-32-2380-232

Received: 7 March 2018; Accepted: 4 April 2018; Published: 7 April 2018



Abstract: The paper presents results of the investigations on the effect of low-temperature thermomechanical treatment (LTTT) on the microstructure of AlZn6Mg0.8Zr alloy (7000 series) and its mechanical properties as well as electrochemical and stress corrosion resistance. For comparison of the LTTT effect, the alloy was subjected to conventional precipitation hardening. Comparative studies were conducted in the fields of metallographic examinations and static tensile tests. It was found that mechanical properties after the LTTT were better in comparison to after conventional heat treatment (CHT). The tested alloy after low-temperature thermomechanical treatment with increasing plastic deformation shows decreased electrochemical corrosion resistance during potentiodynamic tests. The alloy after low-temperature thermomechanical treatment with deformation degree in the range of 10 to 30% is characterized by a high resistance to stress corrosion specified by the level of P_{SCC} indices.

Keywords: aluminium alloy; 7003 alloy; corrosion resistance; thermomechanical treatment; TEM; X-ray diffraction

1. Introduction

The effect of microstructure and morphology of intermetallic phases on mechanical properties and corrosion resistance of Al–Zn–Mg wrought aluminium alloys is important due to the required properties of final products. The proper design of structural elements exposed to the aggressive impact of chloride ion medium requires comprehensive understanding of the relationships between microstructure, microsegregation of alloying elements, type and morphology of intermetallic precipitations, and the heat or thermomechanical treatment performed [1–5]. Refinement of microstructure and the size of precipitations, ensuring optimal strain hardening and precipitation strengthening of the 7000 series aluminium alloys as a result of thermomechanical processing, is an indispensable condition for technological development in the field of newly designed light constructions of machines and devices in many industrial fields [6–9].

Integration of heat treatment and plastic deformation operations of aluminium alloys significantly improves their impact efficiency on the microstructure, especially in the case of conventional techniques

including cold rolling, solution heat treatment, and ageing. Advantageous effects of improved mechanical properties and corrosion resistance of Al–Zn–Mg alloys are obtained as a result of synergetic interactions of strain hardening and precipitation hardening [10–13]. Cold deformation of supersaturated solid solution reduces its thermodynamic stability and accelerates ageing effects. However, the influence of strain hardening on the ageing process is complicated, because it depends on conditions of supersaturation, deformation degree and ageing temperature, alloy type, and the type of precipitations occurring during ageing [14–17].

Nowadays, Al–Zn–Mg–Cu alloys and their various modifications with Zr, Sc, and Ti microadditions are most interesting among the high-strength aluminium alloys of the 7000 series. Deng et al. [11] investigated the possibility of counteracting recrystallization in the 7085 alloy by applying high-temperature thermomechanical treatment with subsequent precipitation hardening. In turn, Lee et al. [12] considered obtaining the fine-grained microstructure of the 7075 alloy using twin roll casting and thermomechanical treatment. Another modification of technological process of the 7075 alloy, which consisted of double thermomechanical processing leading to refinement of the microstructure, was proposed by El-Baradie et al. [13]. Zuo et al. [15–17] used two-stage hot rolling during thermomechanical treatment of the 7055 alloy for realization of the same purpose. In turn, Huo et al. [18,19] carried out continuous rolling during cooling from a hot rolling temperature for the 7075 alloy.

Adequate resistance in aggressive corrosive media is an important criterion in selecting Al–Zn–Mg alloys for responsible construction elements in various industries. Chemical composition becomes substantial in this aspect—primarily the total content of Zn and Mg, the amount of Cu, and microadditions of Zr, Sc, or Ti [20–22]. Moreover, microstructure development, ensuring high stress corrosion resistance while maintaining high mechanical properties, is also not to be neglected [23,24]. Wang et al. [25] investigated the stress corrosion resistance of an Al–Zn–Mg alloy with a small content of additions, subjected to two-stage precipitation hardening. Successively, comprehensive considerations on the effect of variant heat treatment of Al–Zn–Mg–Cu (7085) alloy on microstructure and mechanical properties, and, in particular, resistance to intercrystalline and stress corrosion, were the subject of research led by Peng et al. [26]. The effect of precipitation hardening parameters on microstructure of an Al–Zn–Mg–Sc–Zr alloy, which in turn determines stress corrosion resistance, was undertaken by Huang et al. [27]. Sun et al. [28] conducted research on the dependence of grain boundary structure and stress corrosion of an Al–Zn–Mg alloy without Cu and microadditions.

Available literature data mainly relate to Al–Zn–Mg alloys containing Cu. Difficulties in obtaining high-quality welded joints limit their application. Aluminium alloys of this series, with limited amounts of Cu, are superior in this aspect. There are, however, relatively few scientific studies on these alloys. The number of available publications dealing with the matter of thermomechanical treatment of the 7000 series alloys, and, in particular, its low-temperature variant with Zr microaddition, is also not high. Therefore, the development of knowledge, enabling optimal use of available methods of plastic working and heat treatment as well as their synergetic effect on improvement of functional properties of 7000 series aluminium alloys without the addition of Cu, is desirable. This is why studies of AlZn6Mg0.8Zr alloy were aimed at determining the impact of different reductions during low-temperature thermomechanical treatment on its microstructure, mechanical properties, and resistance to electrochemical and stress corrosion.

2. Materials and Methods

2.1. Materials and Heat Treatment

The material used was a metal sheet, cold-rolled from Al–Zn–Mg (7000 series) commercial aluminium alloy with the following chemical composition: 6.13 Zn, 0.74 Mg, 0.30 Mn, 0.20 Fe, 0.17 Cr, 0.12 Si, 0.08 Zr, 0.04 Cu, and the remainder Al. The investigated alloy was subjected to the following low-temperature thermomechanical treatment: supersaturation in water from the temperature of

500 °C after a holding time of 1 h; cold-rolled with a reduction of 10%, 20%, and 30%; strain-aged for 12 h at a temperature of 150 °C; then cooled down in the open air (Figure 1). For comparison purposes, the tested alloy was subjected to the following precipitation hardening: solution heat treatment (supersaturation) in water from the temperature of 500 °C after a holding time of 1 h; quench-aged for 12 h at a temperature of 150 °C; then cooled down in the open air.

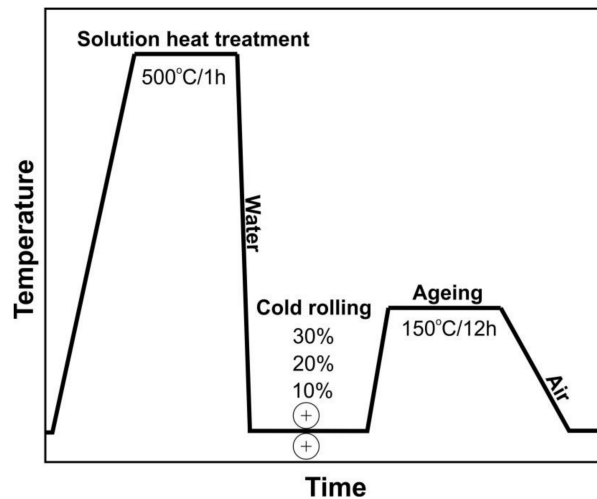


Figure 1. A schematic diagram of the low-temperature thermomechanical treatment (LTTT) of the AlZn6Mg0.8Zr alloy.

2.2. Tensile Test

Static tensile tests of the AlZn6Mg0.8Zr alloy were carried out at room temperature after low-temperature thermomechanical treatment and conventional precipitation hardening using an INSTRON 4505 universal testing machine at a traverse speed rate of 2 mm/min, according to the standard [29]. For examinations of mechanical properties, round samples (three for each state) with the following dimensions of the measuring part were used: \varnothing 10 mm and $l_0 = 60$ mm. The presented results are an arithmetic average of three measurements.

2.3. Transmission Electron Microscopy

Transmission electron microscopy (TEM) tests were carried out using the thin foil technique. Discs of \varnothing 3 mm diameter, cut from the AlZn6Mg0.8Zr alloy after low-temperature thermomechanical treatment (LTTT) and conventional heat treatment (CHT), were ground on abrasive paper to a thickness of about 0.3 mm, and then electrolytically polished at temperature -20 °C at voltage 16.5 V in Struers A2 reagent using a TenuPol-5 device. The microstructure of the thin foils was observed using a TECNAI G2 (FEI) transmission electron microscope, at accelerating voltage of 200 kV and magnification up to $120000\times$. The phase identification procedure, based on electron diffraction, was performed with the aid of the ELDYF computer program [30].

2.4. X-ray Diffraction Examinations

X-ray examinations were performed in the delivery state and after conventional heat treatment and LTTT operations. For this purpose, the D8 Advance (Bruker, Karlsruhe, Germany) X-ray diffractometer was used. The XRD pattern was obtained with the Bragg–Brentano method using X-ray radiation with energy of approximately 8.041 keV, which corresponds to with a wavelength of approximately 1.54184 Å. X-ray qualitative analysis was carried out in the range of θ angles from 10° to 40° . In order to obtain high-quality diffraction patterns of high accuracy and precision, the time of measurement

cycle (step) was set to 100 s, which increases the recording time of one diffraction line ranging from a few to several hours at the step equal to $0.045^\circ \theta$.

2.5. Electrochemical and Stress Corrosion Examinations

Electrochemical corrosion resistance tests were performed using the potentiodynamic method, in accordance with recommendations of the standard [31]. Corrosion resistance was analyzed on the basis of registered potentiodynamic curves of a logarithm dependence of current density versus potential value. Measurements were carried out in the 3.5% NaCl medium (pH = 7). The examinations were performed on three specimens for each state after LTTT and the arithmetic average of measurements is presented.

Stress corrosion resistance tests were executed at the PNA Gdynia stand at a constant tensile load of $\sigma_0 = (0.8)R_{p0.2}$ (yield strength) in the medium of 3.5% NaCl aqueous solution. The corrosion test temperature was within the range of room temperature, and the NaCl aqueous solution was changed every two days. The shape of specimens is presented in Figure 2. The exposure time was equal to 1512 h, and three specimens for each state were used. The resistance of the tested alloy to stress corrosion was determined by comparing mechanical properties obtained in a static tensile test before and after corrosion exposure, using the following Formula (1):

$$P_{SCC} = \left(1 - \frac{P_{NaCl}}{P_{air}}\right) \cdot 100\% \quad (1)$$

where

P_{SCC} —stress corrosion susceptibility index for individual material properties;

P_{NaCl} —material property measured in corroding medium;

P_{air} —material property measured in air.

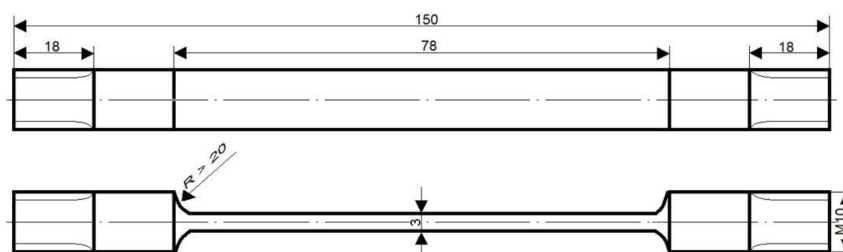


Figure 2. Shape and dimensions of stress corrosion test specimens.

3. Results and Discussion

3.1. Mechanical Properties and Microstructure

The AlZn6Mg0.8Zr alloy subjected to LTTT reveals a yield point from approximately 256 MPa to about 300 MPa and tensile strength from approximately 321 MPa to 347 MPa, depending on the degree of cold deformation after solution heat treatment in a range from 10 to 30% (Figure 3a). The obtained values of tensile strength are lower (approximately 250 MPa) in comparison with an alloy containing 8.38% Zn, 2.07% Mg, 2.31% Cu, and 0.13% Zr subjected to high-temperature thermomechanical treatment (HTTT) [15–17]. However, the strength difference decreases with the reduction of Cu and Zr contents. For example, an alloy containing 7.81% Zn, 1.62% Mg, 1.81% Cu, and 0.13% Zr after HTTT is characterized by 160 MPa higher tensile strength [11], while an alloy with a copper content limited to 0.1% Cu and 0.13% Zr subjected to more complex heat treatment shows a 30 MPa increase in tensile strength [8]. It should be noted that these values depend significantly on processing conditions. The value of the $R_{p0.2}/R_m$ ratio varies along with the deformation degree from 0.8 to 0.87. Elongation of

the examined alloy takes similar values, whereas reduction of area decreases by approximately 9% for a given deformation range (Figure 3b). Obtained values of mechanical properties after thermomechanical treatment are higher when compared to the values obtained after CHT (Table 1). A significant rise in yield point has been noted. Thermomechanical treatment causes a slight decrease of elongation. Nevertheless, in comparison to the alloy subjected to the CHT, the tested alloy subjected to the LTTT is characterized by higher strength and reduction of area in the entire range of deformation.

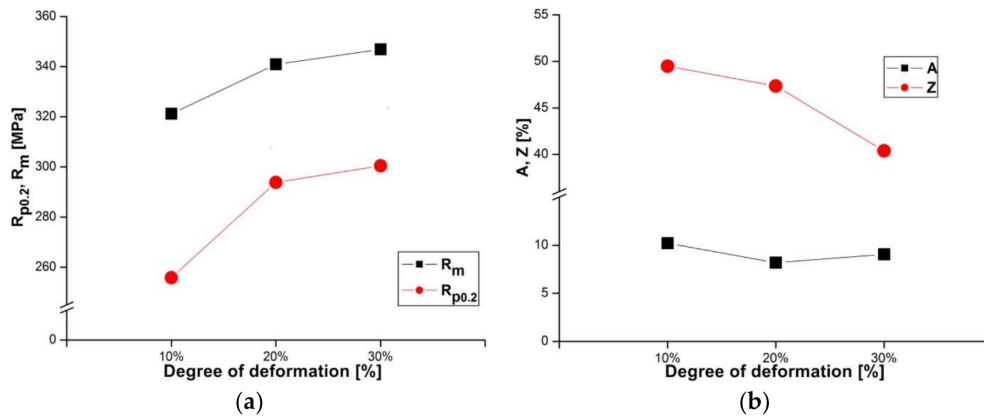


Figure 3. Influence of deformation degree on (a) strength and (b) plastic properties of the investigated alloy after LTTT.

Table 1. Mechanical properties of the investigated alloy after the LTTT and conventional heat treatment (CHT).

Treatment Parameters				Mechanical Properties			
LTTT							
Temperature of Solution Heat Treatment (°C)	Temperature of Ageing (°C)	Time of Ageing (h)	Degree of Deformation (%)	$\bar{R}_{p0.2}$ (MPa)	\bar{R}_m (MPa)	\bar{A} (%)	\bar{Z} (%)
500	150	12	10%	256 ± 4	321 ± 2	10.2 ± 0.4	50 ± 5
			20%	294 ± 2	341 ± 2	8.2 ± 1.1	47 ± 5
			30%	301 ± 2	347 ± 2	9.1 ± 0.9	40 ± 4
CHT							
500	150	12	—	230 ± 3	310 ± 2	16.8 ± 0.5	34 ± 4

R_m —tensile strength; A —total elongation; Z —reduction in area.

The $R_{p0.2}/R_m$ ratio should also be taken into consideration. The AlZn6Mg0.8Zr alloy subjected to LTTT is characterized by a higher $R_{p0.2}/R_m$ ratio (about 0.87), in comparison to the CHT carried out (about 0.74) under comparable processing conditions. Generally, higher values of this ratio are observed for aluminium alloys with a smaller fraction of recrystallized microstructure, higher strengthening from the substructure, and lower elongation [11], which corresponds well with obtained results.

Observations of thin foils using transmission electron microscopy (TEM) revealed after the CHT the substructure of the α solution matrix composed of subgrains ranging from 1 μm to about 2 μm , inside which fine, oval, and nonuniformly distributed precipitates were found (Figure 4a). The presence of grain boundaries with particles arranged along these boundaries (Figure 4b), often in a continuous manner (Figure 4c), was also revealed. These precipitates are also distributed uniformly inside grains or they are stochastic. It has also been found that there are precipitation-free zones (PFZ) in the vicinity of grain boundaries (Figure 4c). This microstructure is characteristic for Al–Zn–Mg alloys subjected to heat treatment [25–27]. Deschamps et al. [9] found that the critical factor shaping the microstructure of Al–Zn–Mg–Zr alloys, in addition to degradation and morphology of the Al_3Zr phase, is also the volume fraction of GP zones, because they are privileged nucleation areas of the

η' phase. Electron diffractions revealed reflexes coming from the α solution matrix (Al) and MgZn_2 phase (Figure 5).

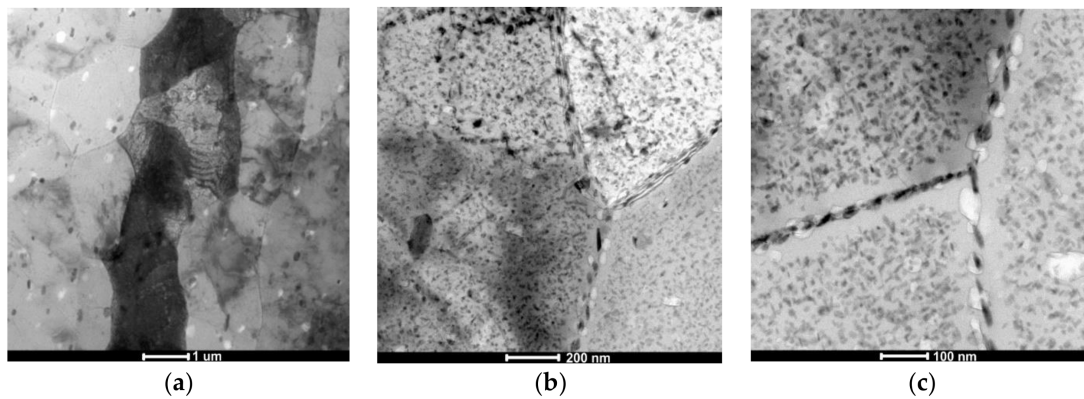


Figure 4. The AlZn6Mg0.8Zr alloy after CHT: (a) substructure; (b) precipitations inside grains and along grains' boundaries; (c) precipitation-free zones (PFZ) near to grains' boundaries with continuously distributed precipitates.

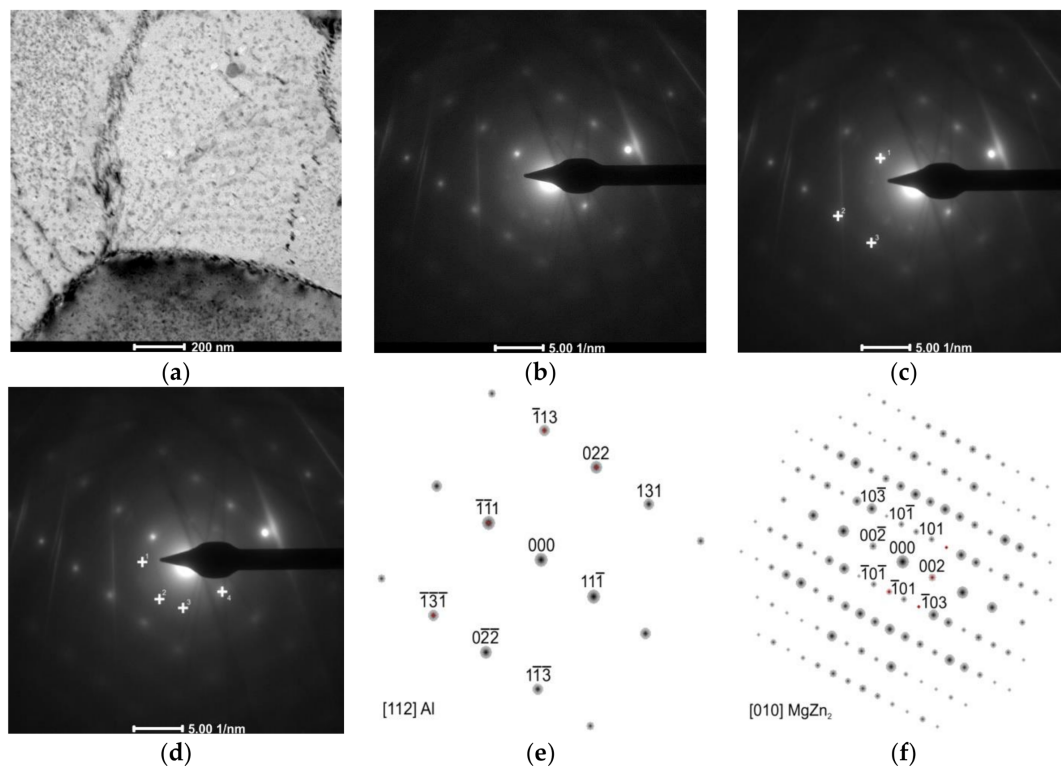


Figure 5. The AlZn6Mg0.8Zr alloy after CHT: (a) substructure of investigated alloy with stochastic distribution of precipitations inside subgrains and along their boundaries; (b) electron diffraction; (c) marked reflections of α solution matrix; (d) marked reflections of MgZn_2 particle; (e) solution of α phase matrix diffraction and (f) solution of MgZn_2 phase diffraction.

The alloy subjected to the LTTT with 10% reduction is characterized by the microstructure composed of subgrains of the α solution with size in the range of 0.5–1 μm (Figure 6a). Fine, oval precipitates are usually distributed along grain boundaries (Figure 6b). They do not form continuous nets. Along these boundaries, a narrow precipitation-free zone can be observed—less distinct than in

precipitates. This is the result of the formation of a higher density of dislocations in the supersaturated α solution, which not only accelerate disintegration of this solution, but act as preferred nucleation areas of precipitation even before accelerated ageing during deformation, in the process of dynamic strain ageing and as an effect of hereditary impact—so-called static strain ageing—while soaking the alloy at the ageing temperature [15]. This is due to an increased diffusion rate in these processes and the presence of numerous nuclei in the deformed α solution, as well as faster coagulation of these phases. Similar results of the impact of plastic deformation on the microstructure of Al–Zn–Mg-type alloys have been presented in the literature [16–19]. The discussed changes in microstructure significantly affect obtained mechanical properties and, in particular, the dependencies between the level of strength and plastic properties [33,34]. On the one hand, attention is paid to the impact of the increased amount of precipitates formed in the LTTT process on the level of alloy strengthening. On the other hand, it influences a morphology, especially the degree of coagulation and distribution of formed particles. They affect a higher level of reduction in area after the LTTT compared with after conventional heat treatment.

3.2. Precipitation Behavior

Qualitative phase analysis of the AlZn6Mg0.8Zr alloy after the ageing stage in the CHT process revealed diffraction reflexes from the α matrix (Al) and Al₃Zr and MgZn₂ phases (Figure 10a). The same phases were identified in the alloy subjected to 30% cold deformation (Figure 10b). Moreover, the analysis of the intensity of recorded diffraction lines of the α solution matrix (Al), especially in case of the LTTT, indicates the lack of their compatibility with standard data.

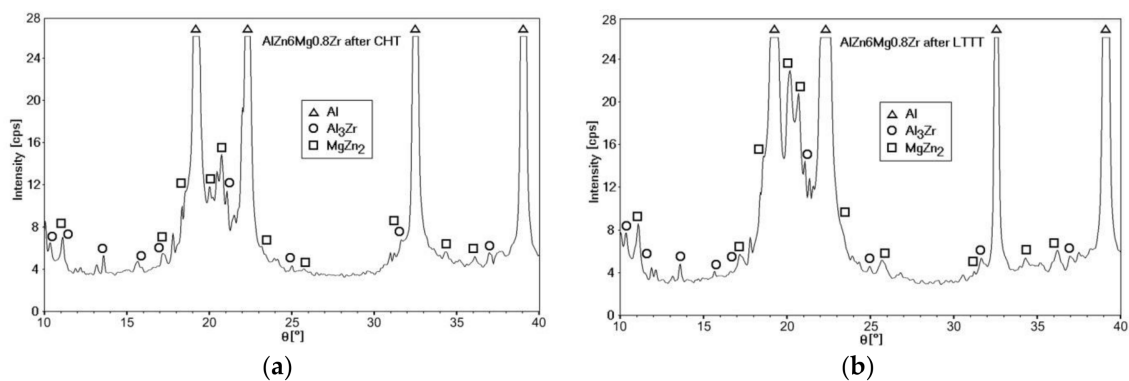


Figure 10. XRD patterns of the AlZn6Mg0.8Zr alloy after: (a) CHT ($T_s = 500\text{ }^\circ\text{C}$; $T_a = 150\text{ }^\circ\text{C}$; $\tau_a = 12\text{h}$); (b) LTTT ($T_s = 500\text{ }^\circ\text{C}$; 30%; $T_a = 150\text{ }^\circ\text{C}$; $\tau_a = 12\text{h}$).

The MgZn₂ phase is most often identified by X-ray phase analysis [15,19,21,25]. Extending the time of the measurement step to 100s allowed the obtaining of more accurate diffraction patterns, which enabled the identification of Al₃Zr dispersoids. The presence of fine-dispersive Al₃Zr phases in alloys of the 7000 series, which are formed already during cooling of the alloy after solution heat treatment, is important because they can become privileged areas of heterogeneous nucleation of the strengthening η -MgZn₂ phase [7]. The occurrence of Al₃Zr particles in combination with the high dislocation density, in the case of the LTTT processing, causes formation of more nucleation sites for the η phase and, thus, a higher strength of alloys containing Zr [9,11].

3.3. Corrosion Resistance

The AlZn6Mg0.8Zr alloy subjected to the LTTT with 10% and 20% reductions has a comparable corrosion potential (approximately -830 mV) (Figure 11). An increase in degree of deformation to 30% causes a decrease in E_{cor} by approximately 35 mV toward more active values. The value of the I_{cor} index increases and R_p decreases along with the increase of the deformation (Table 2). It was found that

increase of the deformation amount leads to a decrease of electrochemical corrosion resistance. This is due to the formation of larger fraction of precipitates. They interact with the matrix and undergo anodic stripping, leading to the deterioration of electrochemical pitting corrosion factors [21,22,28].

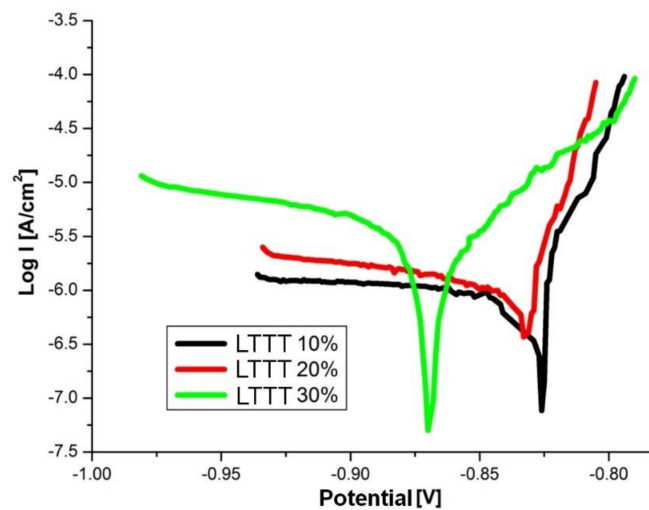


Figure 11. Polarization curves of the alloy after the LTTT with plastic deformation of 10%, 20%, and 30%.

Table 2. Electrochemical parameters obtained from cyclic polarization measurements.

Degree of Deformation (%)	E_{cor} (mV)	I_{cor} ($\mu\text{A}/\text{cm}^2$)	R_p ($\text{k}\Omega$)
10	-830 ± 1	0.30 ± 0.2	17.4 ± 0.5
20	-833 ± 3	1.32 ± 0.3	6.2 ± 0.2
30	-867 ± 4	11.17 ± 0.7	5.4 ± 0.9

The alloy subjected to the LTTT is characterized by a slight decrease in mechanical properties in a static tensile test after loading the samples under stress corrosion conditions (Table 3). It was found that the decrease of mechanical factors after stress and corrosion exposures of samples is reduced when the degree of deformation rises. High values of stress corrosion susceptibility indices of the tested alloy (P_{SCC}) allow us to state that the AlZn6Mg0.8Zr alloy, subjected to the LTTT, is not very susceptible to this type of corrosion (Table 4). Similar conclusions for an Al–Zn–Mg–Zr alloy containing a small amount of Cu, subjected to various conventional heat treatments, were obtained by Xiao et al. [8]. In their case, the decrease in mechanical properties was more pronounced. It was also observed that P_{SCC} indices, for certain strength properties, are smaller than plastic properties indices (Z_{SCC} in particular). This indicates that strength properties are less susceptible to the effects of stress corrosion conditions. A decrease in all P_{SCC} indexes was also noted along with an increase in the deformation degree, which reflects improved stress corrosion resistance of the alloy along with its strengthening.

Cold deformation after solution heat treatment results in formation of a dislocation network, providing privileged areas for heterogeneous nucleation of the η phase. Moreover, new diffusion paths are created, which affect the precipitation sequence of the strengthening phases. As a consequence, the amount of η phase formed in the deformed alloy is larger than the portion of η' phase, which positively influences the resistance under stress corrosion conditions [24]. Moreover, ageing activated diffusion of alloying elements from inside to grain boundaries of cold-deformed alloys. This results in growth and coagulation of precipitates at the boundaries and their distribution in large intervals between them. The precipitation-free zone is also reduced [25–27,35].

Table 3. Mechanical properties of AlZnMg0.8Zr alloy, subjected to LTTT, obtained after and before stress corrosion tests.

Degree of Deformation (%)	$\overline{R}_{p0.2}$ (MPa)	\overline{R}_m (MPa)	\overline{A} (%)	\overline{Z} (%)
Before Corrosion				
10	256 ± 4	321 ± 2	10.2 ± 0.4	50 ± 5
20	294 ± 2	341 ± 2	8.2 ± 1.1	47 ± 5
30	301 ± 2	347 ± 2	9.1 ± 0.9	40 ± 4
After Corrosion				
10	249 ± 2	316 ± 2	9.8 ± 1.3	46 ± 3
20	289 ± 3	337 ± 3	8.0 ± 0.7	45 ± 5
30	300 ± 4	346 ± 4	8.9 ± 0.5	39 ± 5

Table 4. P_{SCC} indices for the investigated alloy after LTTT.

Degree of Deformation (%)	P _{SCC} Index (%)			
	R _{p0.2SCC}	R _{mSCC}	A _{SCC}	Z _{SCC}
10	2.7	1.7	3.9	7.9
20	1.7	1.1	2.4	5.5
30	0.2	0.2	2.2	4.7

4. Conclusions

Studies of mechanical properties and corrosion resistance of the 7003 series Al–Zn–Mg-type alloy and metallographic analyses lead to the following conclusions:

- Low-temperature thermomechanical treatment with 30% reduction after solution heat treatment in water from the temperature of 500 °C and with ageing at the temperature of 150 °C ensures higher mechanical properties of the alloy in comparison to CHT.
- AlZn6Mg0.8Zr alloy reveals a microstructure consisting of the α solution matrix and fine-dispersive particles of morphologically differentiated intermetallic phases of the Al₃Zr and η -MgZn₂ types. Increase of cold deformation results in obtaining a smaller precipitation-free zone after ageing and formation of a greater portion of strengthening phases in the vicinity of grain boundaries. This affects the increase in the distance between precipitates located at grain boundaries.
- Electrochemical corrosion resistance of the AlZn6Mg0.8Zr alloy in the 3.5% NaCl medium decreases along with increasing plastic deformation degree, whereas the opposite behavior occurs in the case of stress corrosion resistance, which is improved. This is related to complex microstructural phenomena, which must be studied in more detail.

Author Contributions: A.K. and W.O. conceived and designed the experiments; A.K. performed tensile tests, analyzed the data and wrote the paper; W.O. supervised the work; W.J. performed stress corrosion examinations; A.G. analyzed the data and reviewed the paper; S.B. performed TEM experiments and analyzed the results; J.Ž. performed X-ray diffraction examinations and analyzed the results; All authors discussed the paper.

Conflicts of Interest: The authors declare no conflict of interest.

References

1. Hyde, K.B.; Norman, A.F.; Prangnell, P.B. The effect of cooling rate on the morphology of primary Al₃Sc inter-metallic particles in Al–Sc alloys. *Acta Mater.* **2001**, *49*, 1327–1337. [[CrossRef](#)]
2. Davydov, V.G.; Rostova, T.D.; Zakharov, V.V.; Filatov, Yu.A.; Yelagin, V.I. Scientific principles of making an alloying addition of scandium to aluminium alloys. *Mater. Sci. Eng. A* **2000**, *280*, 30–36. [[CrossRef](#)]
3. Chen, G.; Zhang, Y.; Du, Z. Mechanical behavior of Al–Zn–Mg–Cu alloy under tension in semi-solid state. *Trans. Nonferrous Met. Soc. China* **2016**, *26*, 643–648. [[CrossRef](#)]

4. Khalid Rafi, H.; Janaki Ram, G.D.; Phanikumar, G.; Prasad Rao, K. Microstructure and tensile properties of friction welded aluminium alloy AA7075-T6. *Mater. Design* **2010**, *31*, 2375–2380. [[CrossRef](#)]
5. Fuller, C.B.; Krause, A.R.; Dunand, D.C.; Seidman, D.N. Microstructure and mechanical properties of a 5754 aluminum alloy modified by Sc and Zr additions. *Mater. Sci. Eng. A* **2002**, *338*, 8–16. [[CrossRef](#)]
6. Xiang, H.; Pan, Q.L.; Yu, X.H.; Huang, X.; Sun, X.; Wang, X.D.; Li, M.J. Superplasticity behaviors of Al-Zn-Mg-Zr cold-rolled alloy sheet with minor Sc addition. *Mater. Sci. Eng. A* **2016**, *676*, 128–137. [[CrossRef](#)]
7. Lü, X.; Guo, E.; Rometsch, P.; Wang, L. Effect of on-step and two-step homogenization treatments on distribution of Al₃Zr dispersoids in commercial AA7150 aluminium alloy. *Trans. Nonferrous Met. Soc. China* **2012**, *22*, 2645–2651. [[CrossRef](#)]
8. Xiao, T.; Deng, Y.; Ye, L.; Lin, H.; Shan, Ch.; Qian, P. Effect of three-stage homogenization on mechanical properties and stress corrosion cracking of Al-Zn-Mg-Zr alloys. *Mater. Sci. Eng. A* **2016**, *675*, 280–288. [[CrossRef](#)]
9. Deschamps, A.; Bréchet, Y. Influence of quench and heating rates on the ageing response of an Al-Zn-Mg-(Zr) alloy. *Mater. Sci. Eng. A* **1998**, *251*, 200–207. [[CrossRef](#)]
10. Kowalski, A.; Ozgowicz, W.; Grajcar, A.; Lech-Grega, M.; Kurek, A. Microstructure and Fatigue Properties of AlZn6Mg0.8Zr Alloy Subjected to Low-Temperature Thermomechanical Processing. *Metals*, **2017**, *7*, 488. [[CrossRef](#)]
11. Deng, Y.; Zhang, Y.; Wan, L.; Zhang, X. Effect of thermomechanical processing on production of Al-Zn-Mg-Cu alloy plate. *Mat. Sci. Eng. A* **2012**, *554*, 33–40. [[CrossRef](#)]
12. Lee, Y.; Kim, W.; Jo, D.; Lim, Ch.; Kim, H. Recrystallization behavior of cold rolled Al-Zn-Mg-Cu fabricated by twin roll casting. *Trans. Nonferrous Met. Soc. China* **2014**, *24*, 2226–2231. [[CrossRef](#)]
13. El-Baradie, Z.M.; El-Sayed, M. Effect of double thermomechanical treatments on the properties of 7075 Al alloy. *J. Mater. Process. Tech.* **1996**, *62*, 76–80. [[CrossRef](#)]
14. Ozgowicz, W.; Kalinowska, E.; Kowalski, A.; Gołombek, K. The structure and mechanical properties of Al-Mg-Mn alloys shaped in the process of thermomechanical treatment. *J. Achiev. Mater. Manuf. Eng.* **2011**, *45*, 148–156.
15. Zuo, J.; Hou, L.; Shi, J.; Cui, H.; Zhuang, L.; Zhang, J. The mechanism of grain refinement and plasticity enhancement by an improved thermomechanical treatment of 7055 Al alloy. *Mat. Sci. Eng. A* **2017**, *702*, 42–52. [[CrossRef](#)]
16. Zuo, J.; Hou, L.; Shi, J.; Cui, H.; Zhuang, L.; Zhang, J. Effect of deformation induced precipitation on grain refinement and improvement of mechanical properties AA 7055 aluminum alloy. *Mater. Charact.* **2017**, *130*, 123–134. [[CrossRef](#)]
17. Zuo, J.; Hou, L.; Shi, J.; Cui, H.; Zhuang, L. Enhanced plasticity and corrosion resistance of high strength Al-Zn-Mg-Cu alloy processed by an improved thermomechanical processing. *J. Alloy Compd.* **2017**, *716*, 220–230. [[CrossRef](#)]
18. Huo, W.T.; Shi, J.T.; Hou, L.G.; Zhang, J.S. An improved thermo-mechanical treatment of high-strength Al-Zn-Mg-Cu alloy for effective grain refinement and ductility modification. *J. Mater. Process. Tech.* **2017**, *239*, 303–3014. [[CrossRef](#)]
19. Huo, W.; Hou, L.; Cui, H.; Zhuang, L.; Zhang, J. Fine-grained AA 7075 processed by different thermo-mechanical processings. *Mat. Sci. Eng. A* **2014**, *618*, 244–253. [[CrossRef](#)]
20. Segal, V.M. New hot thermo-mechanical processing of heat treatable aluminum alloys. *J. Mater. Process. Tech.* **2016**, *231*, 50–57. [[CrossRef](#)]
21. Navaser, M.; Atapour, M. Effect of friction stir processing on pitting corrosion and intergranular attack of 7075 aluminum alloy. *J. Mater. Sci. Technol.* **2017**, *33*, 155–165. [[CrossRef](#)]
22. Li, S.; Guo, D.; Dong, H. Effect of flame rectification on corrosion property of Al-Zn-Mg alloy. *Trans. Nonferrous Met. Soc. China* **2017**, *27*, 250–257. [[CrossRef](#)]
23. Lu, X.; Han, X.; Du, Z.; Wang, G.; Lu, L.; Lei, J.; Zhou, T. Effect of microstructure on exfoliation corrosion resistance in an Al-Zn-Mg alloy. *Mater. Charact.* **2018**, *135*, 167–174. [[CrossRef](#)]
24. Umamaheshwer Rao, A.C.; Vasu, V.; Govindaraju, M.; Sai Srinadh, K.V. Stress corrosion cracking behavior of 7xxx aluminum alloys: A literature review. *Trans. Nonferrous Met. Soc. China* **2016**, *26*, 1447–1471.
25. Wang, Y.L.; Jiang, H.C.; Li, Z.M.; Yan, D.S.; Zhang, D.; Rong, L.J. Two-stage double peaks ageing and its effect on stress corrosion cracking susceptibility of Al-Zn-Mg alloy. *J. Mater. Sci. Technol.* (in press). [[CrossRef](#)]

26. Peng, X.; Guo, Q.; Liang, X.; Deng, Y.; Gu, Y.; Xu, G.; Yin, Z. Mechanical properties, corrosion behavior and microstructures of a non-isothermal ageing treated Al-Zn-Mg-Cu alloy. *Mat. Sci. Eng. A* **2017**, *688*, 146–154. [[CrossRef](#)]
27. Huang, X.; Pan, Q.; Li, B.; Liu, Z.; Huang, Z.; Yin, Z. Microstructure, mechanical properties and stress corrosion cracking of Al-Zn-Mg-Zr alloy sheet with trace amount of Sc. *J. Alloy Compd.* **2015**, *650*, 805–820. [[CrossRef](#)]
28. Sun, X.Y.; Zhang, B.; Lin, H.Q.; Zhou, Y.; Sun, L.; Wang, J.Q.; Han, E.-H.; Ke, W. Correlations between stress corrosion cracking susceptibility and grain boundary microstructures for an Al-Zn-Mg alloy. *Corros. Sci.* **2013**, *77*, 103–112. [[CrossRef](#)]
29. ISO 6892-1:2016. *Metallic Materials—Tensile Testing—Part 1: Method of Test at Room Temperature*; Chinese Code: Beijing, China, 2010.
30. Gigla, M.; Paćzkowski, P. The computer aided analysis of electron diffraction patterns. *Arch. Mater. Sci.* **2006**, *1*, 49–69.
31. ISO 17475:2015. *Corrosion of Metals and Alloys—Electrochemical Test Methods—Guidelines for Conducting Potentiostatic and Potentiodynamic Polarization Measurements*; Chinese Code: Beijing, China, 2010.
32. Ozgowicz, W. *Physicochemical, Structural and Mechanical Factors of Intergranular Brittleness of the α Bronzes at Elevated Temperature*; Scientific Notebooks of Silesian University of Technology: Gliwice, Poland, 2004.
33. Han, N.; Zhang, X.; Liu, S.; Ke, B.; Xin, X. Effects of pre-stretching and ageing on the strength and fracture toughness of aluminum alloy 7050. *Mat. Sci. Eng. A* **2011**, *528*, 3714–3721. [[CrossRef](#)]
34. Srivatsan, T.S.; Sriram, S.; Veeraraghavan, D.; Vasudevan, V.K. Microstructure, tensile deformation and fracture behaviour of aluminium alloy 7055. *J. Mater. Sci.* **1997**, *32*, 2883–2894. [[CrossRef](#)]
35. Wang, D.; Ma, Z.Y.; Gao, Z.M. Effect of severe cold rolling on tensile properties and stress corrosion cracking of 7050 aluminum alloy. *Mater. Chem. Phys.* **2009**, *17*, 228–233. [[CrossRef](#)]



© 2018 by the authors. Licensee MDPI, Basel, Switzerland. This article is an open access article distributed under the terms and conditions of the Creative Commons Attribution (CC BY) license (<http://creativecommons.org/licenses/by/4.0/>).